Monthly Notices
of the
ROYAL ASTRONOMICAL SOCIETY

MNRAS **470,** 4231–4240 (2017)
Advance Access publication 2017 June 9

doi:10.1093/mnras/stx1440

A Universe of ultradiffuse galaxies: theoretical predictions from ΛCDM simulations

Yu Rong,[1]★ Qi Guo,[1] Liang Gao,[1,2] Shihong Liao,[1] Lizhi Xie,[3] Thomas H. Puzia,[4] Shuangpeng Sun[1] and Jun Pan[1]

[1]*Key Laboratory for Computational Astrophysics, The Partner Group of Max Planck Institute for Astrophysics, National Astronomical Observatories, Chinese Academy of Sciences, Beijing 100012, China*
[2]*Department of Physics, Institute of Computational Cosmology, University of Durham, Science Laboratories, South Road, Durham DH1 3LE, UK*
[3]*OATS, INAF, Via Bazzoni 2, I-34124-Trieste, TS, Italy*
[4]*Instituto de Astrofísica, Pontificia Universidad Católica de Chile, Av. Vicuña Mackenna 4860, 7820436 Macul, Santiago, Chile*

Accepted 2017 June 7. Received 2017 June 7; in original form 2017 March 23

ABSTRACT

A particular population of galaxies have drawn much interest recently, which are as faint as typical dwarf galaxies but have the sizes as large as L^* galaxies, the so called ultradiffuse galaxies (UDGs). The lack of tidal features of UDGs in dense environments suggests that their host haloes are perhaps as massive as that of the Milky Way. On the other hand, galaxy formation efficiency should be much higher in the haloes of such masses. Here, we use the model galaxy catalogue generated by populating two large simulations: the Millennium-II cosmological simulation and Phoenix simulations of nine big clusters with the semi-analytic galaxy formation model. This model reproduces remarkably well the observed properties of UDGs in the nearby clusters, including the abundance, profile, colour and morphology, etc. We search for UDG candidates using the public data and find two UDG candidates in our Local Group and 23 in our Local Volume, in excellent agreement with the model predictions. We demonstrate that UDGs are genuine dwarf galaxies, formed in the haloes of $\sim 10^{10}\,M_{\odot}$. It is the combination of the late formation time and high spins of the host haloes that results in the spatially extended feature of this particular population. The lack of tidal disruption features of UDGs in clusters can also be explained by their late infall-time.

Key words: methods: numerical – galaxies: evolution – galaxies: stellar content.

1 INTRODUCTION

A population of low surface brightness galaxies has been observed in spatial regions of, e.g. Coma (Koda et al. 2015; van Dokkum et al. 2015a,b; Yagi et al. 2016), Virgo (Mihos et al. 2015), Fornax (Muñoz et al. 2015), A168 (Román & Trujillo 2017a), A2744 (Janssens et al. 2017), eight other clusters with redshifts $z \sim 0.044$–0.063 (van der Burg, Muzzin & Hoekstra 2016) and Pisces-Perseus supercluster (Martinez-Delgado et al. 2016), as well as several galaxy groups (Makarov et al. 2015; Toloba et al. 2016; Román & Trujillo 2017b; Trujillo et al. 2017). While their stellar masses are similar to typical dwarf galaxies, their effective radii are similar to the L^* galaxies (van Dokkum et al. 2015a; Beasley et al. 2016). These galaxies are generally referred to as ultradiffuse galaxies (UDGs). Except for several blue ones (e.g. Román & Trujillo 2017a), the majority of the observed UDGs populate the red sequence, suggesting that the star formation in UDGs has been quenched before $z \sim 2$ (van der Burg et al. 2016).

UDGs are ubiquitously distributed from the cores of galaxy clusters to the surrounding large-scale filaments (Koda et al. 2015; Román & Trujillo 2017a,b; Yagi et al. 2016). Since they can withstand the strong tidal forces in the cluster cores without significant features of tidal disruption, one scenario is that UDGs are dark-matter-dominated galaxies, for instance, the failed $L_\star$ galaxies that lost their gas content after the first generation of stars (Scannapieco et al. 2008; Stinson et al. 2013; Trujillo-Gomez et al. 2015; van Dokkum et al. 2015a). Using stellar kinematics of Dragonfly 44, van Dokkum et al. (2016) measured its dynamical mass as $\sim 10^{12}\,M_{\odot}$, similar to the mass of the Milky Way; this is unexpected from prediction of subhalo abundance matching (SHAM) in which galaxy formation efficiency reaches its maximum at this halo mass (Conroy & Wechsler 2009; Guo et al. 2010; Simha et al. 2012). Another scenario is that UDGs are spatially extended dwarf galaxies (e.g. Dalcanton et al. 1997a; Dalcanton, Spergel & Summers 1997b; Mo, Mao & White 1998; Huang et al. 2012; Amorisco & Loeb 2016; Di Cintio et al. 2017). Using the abundance and kinematics of

★ E-mail: rongyuastrophysics@gmail.com

globular clusters around two UDGs, VCC 1287 and DF17, Beasley et al. (2016) and Beasley & Trujillo (2016) estimated the corresponding dynamical masses to be around $m_{\rm vir} \sim (8 \pm 4) \times 10^{10}\,{\rm M}_{\odot}$ and $m_{\rm vir} \sim (9 \pm 2) \times 10^{10}\,{\rm M}_{\odot}$, respectively, similar to that of the typical dwarf galaxies. Using the relation between the mass of the globular cluster system and the halo mass (Harris, Harris & Alessi 2013; Harris, Harris & Hudson 2015), Peng & Sungsoon (2016) also inferred the total mass of DF17 to be $(9.3 \pm 4.7) \times 10^{10}\,{\rm M}_{\odot}$; Amorisco, Monachesi & White (2016) estimated the dynamical masses of 54 Coma UDGs to be lower than $1.3 \times 10^{11}\,{\rm M}_{\odot}$. Román & Trujillo (2017a) also found that the distribution of UDGs around A168 is similar to the normal dwarfs, but significantly different from the distribution of massive galaxies with masses similar to the Milky Way. Using the width of the H I line, Trujillo et al. (2017) found a UDG in the very local Universe with a virial mass of $8 \times 10^{10}\,{\rm M}_{\odot}$. Theoretical work also suggests that UDGs might be genuine dwarf galaxies possibly with high spins (Yozin & Bekki 2015; Amorisco & Loeb 2016), or spatially extended stellar components caused by feedback-driven gas outflows (Di Cintio et al. 2017).

In this paper, we will use a publicly available semi-analytic galaxy catalogue (Guo et al. 2013) to investigate whether UDGs can naturally emerge from the Λ cold dark matter (CDM) hierarchical structure formation model. In Section 2, we briefly describe the simulation and the semi-analytic models, as well as the selection criteria of the possible UDGs. In Section 3, we compare the model predictions with observational results. In Section 4, we study the distributions of the model UDGs, and dependence of UDG properties on environments. In Section 5, we investigate the origin of this particular population. Conclusions are presented in Section 6.

2 UDG SELECTION FROM SIMULATIONS

2.1 Simulations

The galaxy catalogues used here are based on two simulations, the Millennium-II simulation (MS-II; Boylan-Kolchin et al. 2009) and Phoenix simulation (Gao et al. 2012). MS-II is a high-resolution cosmological N-body simulations, following 2160^3 particles from $z = 127$ to 0 in a periodic box of $100\,{\rm Mpc}\,h^{-1}$ on a side. Each dark matter particle has a mass of $6.88 \times 10^6\,{\rm M}_{\odot}\,h^{-1}$. Particle data were stored at 68 logarithmically spaced output times. The MS-II simulation adopted the cosmological parameters consistent with the first-yr *Wilkinson Microwave Anisotropy Probe* (*WMAP*) result; it was then rescaled to that consistent with *WMAP* seven-yr parameters (Guo et al. 2013): $\Omega_{\rm m} = 0.272$, $\Omega_{\rm b} = 0.0455$, $h = 0.704$, $\sigma_8 = 0.81$ and $n = 0.967$. The Phoenix simulation is a high-resolution re-simulation of nine individual rich clusters and their surroundings. Each Phoenix cluster has been simulated at different resolution levels for numerical convergence studies. Here, we adopt the simulation with level 2 resolution. Particle mass is of $\sim 10^6\,{\rm M}_{\odot}\,h^{-1}$, which varies from cluster to cluster slightly. The Phoenix simulation adopted cosmological parameters from a combination of Two-degree-Field Galaxy Redshift Survey (Colless et al. 2001) and first-yr *WMAP* data (Spergel et al. 2003): $\Omega_{\rm m} = 0.25$, $\Omega_{\rm b} = 0.045$, $h = 0.73$, $\sigma_8 = 0.9$ and $n = 1$. Although the cosmological parameters adopted by these two simulations are slightly different, this has negligible effect on our main results.

At each snapshot, dark matter haloes are identified with the friends-of-friends group algorithm by linking particles separated by 0.2 times the mean interparticle separation (Davis et al. 1985). The SUBFIND algorithm (Springel et al. 2001) was then used to identify self-bound subhaloes; merger trees were constructed by linking each subhalo at different output times to its unique descendant using the algorithm described in Springel et al. (2005) and Boylan-Kolchin et al. (2009).

MS-II contains millions of haloes from 10^{10} to $10^{14}\,{\rm M}_{\odot}\,h^{-1}$, allowing us to study the possible UDGs in different environments in a statistical way. Yet limited by the box size, MS-II has no clusters as massive as the Coma clusters, $\sim 2 \times 10^{15}\,{\rm M}_{\odot}$, and A2744, $\sim 5 \times 10^{15}\,{\rm M}_{\odot}$, where the largest samples of UDGs are discovered. The Phoenix simulation suits compensate this by providing more massive cluster samples, and the largest cluster in the Phoenix suits has a mass $\sim 3.4 \times 10^{15}\,{\rm M}_{\odot}$ (at $z = 0$). The minimum resolved halo in this Phoenix cluster is of mass $3.6 \times 10^8\,{\rm M}_{\odot}\,h^{-1}$, well below the mass limit ($\sim 10^9\,{\rm M}_{\odot}$) below which haloes cannot form any galaxies. We thus use the combination of these two simulation sets to study UDGs in various environments.

2.2 Galaxy formation model

In order to populate dark matter haloes with galaxies, we applied the semi-analytic galaxy formation models (Guo et al. 2011, 2013) to the stored subhaloes merger trees extracted from these N-body simulations. This model has been proved successful in reproducing many galaxies properties both in the local Universe and at high redshifts, and particularly it provides convincing results for galaxy size versus stellar mass relations. Here, we briefly summarize the main physical processes relevant to the formation of galaxies as faint as UDGs and the models of galaxy stellar component sizes.

As discussed in Guo et al. (2011; hereafter Guo11), two processes are crucial for the formation of low-mass galaxies: UV reionization and supernova (SN) feedback. The capability to capture baryons is reduced in low-mass systems due to the UV reionization. Guo11 and Guo et al. (2013) adopted results given by Okamoto, Gao & Theuns (2008) to quantify the fraction of baryons as a function of halo mass. As demonstrated in Guo11, this effect becomes significant for galaxies less luminous than $M_V = -11$. Vast amount of energy is released during SN explosion that can reheat the surrounding gas and even eject gas out of its dark halo. Guo11 introduced an SN feedback model that depends on the maximum velocity of the host halo, leading to a relatively more efficient feedback in low-mass haloes than their high-mass counterparts. This significantly changes the slope of the stellar mass function at the low mass end (e.g. stellar mass $m_{\rm st} < 10^{9.5}\,{\rm M}_{\odot}$).

Guo11 uses the stellar population synthesis models from Bruzual & Charlot (2003), and adopts a Chabrier initial function to calculate the photometric properties of galaxies. For low-redshift galaxies, the slab dust model introduced in De Lucia & Blaizot (2007) is then implemented to account for the extinction of star light. Further comparison with observations suggests that the fiducial model of Guo11 can well predict the luminosity function of galaxies at low redshifts (Guo11; Nierenberg et al. 2012), particularly in the faint end.

Our model galaxies contain two components, discs and bulges. Guo11 assumed the stellar disc to have an exponential surface density profile. Its size is determined by the specific angular momentum and the circular velocity (here using $V_{\rm max}$ as a proxy). The angular momentum is obtained from its gas disc during the star formation. The gas disc acquires its angular momentum during the cooling process, i.e. the cooling gas is assumed to have the same specific angular momentum as its host halo. Bulges are formed by mergers and disc instability. In Guo11, bulge sizes were calculated by assuming energy conservation and virial equilibrium. For mergers, the relevant components are the binding energy and interaction

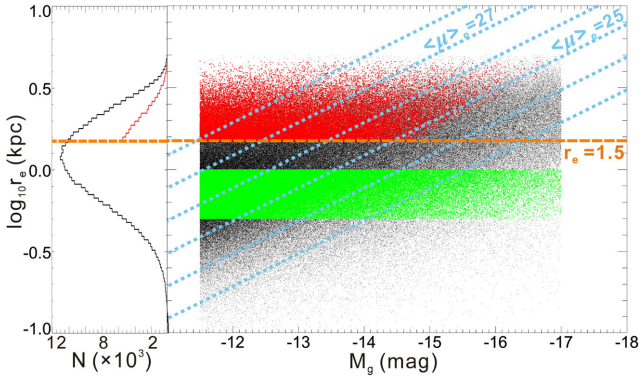

Figure 1. Left-hand panel: r_e distribution for model dwarf galaxies (black histogram) and UDGs (red histogram). Right-hand panel: r_e–M_g relation for model galaxies. Model UDGs with $r_e \in (1.5, 4.6)$ kpc, $M_g \in (-17, -11.5)$ mag, and $\mu_0 > 23.5$ mag arcsec^{-2} are denoted by the red points. Green points mark the dwarf counterparts with $r_e \in (0.1, 1.5)$ kpc, $M_g \in (-17, -11.5)$ mag. Blue tilted dotted lines show the different mean surface brightness thresholds, and the orange horizontal dashed line denotes the threshold of $r_e = 1.5$ kpc.

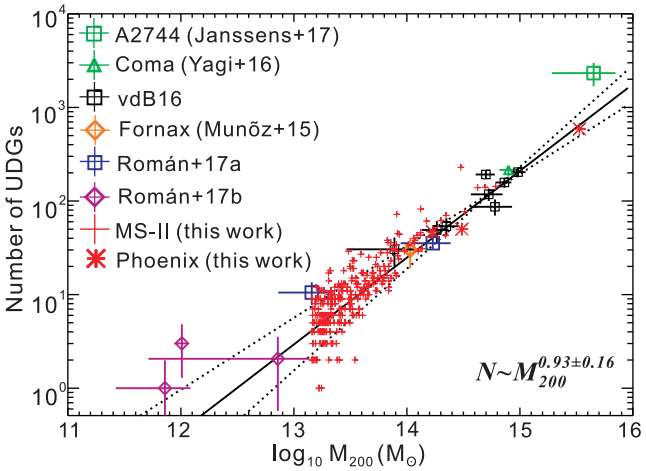

Figure 2. Abundance of UDGs as a function of their host cluster mass. Solid and dashed lines reveal the relation $N \propto M_{200}^{0.93\pm0.16}$ obtained by Janssens et al. (2017). The red crosses and stars show the model predictions in MS-II and Phoenix simulations, respectively, while the other coloured symbols show the abundances of the observed UDGs in clusters and groups.

energy of the two merging galaxies. For disc instability, they are the binding energy and interaction energy of the existing bulges and the part of mass that is transferred into bulges during disc instability.

In order to compare with the observations directly, we convert the 3D radius of our model galaxies to effective radius r_e (also referred to as the projected half-mass radius) by assuming the stellar bulge and stellar disc to have the Jaffe (Jaffe 1983) and exponential density profiles, respectively (see Xie et al. 2015 for details). For each galaxy, we divide its projected radius (from 10 pc to 10 kpc) into 100 bins (r_i, where i is from 1 to 100) in logarithm scale and calculate the projected absolute magnitude $M_i^{\rm pro}$ of each bin. The central surface brightness μ_0 is obtained by fitting the surface brightness $\mu_i \sim M_i^{\rm pro} + 2.5\log_{10}(s_i)$, where s_i is the area of the bin, using a Sérsic model. We test the dependence of our results on bin sizes and find that this effect is minor.

2.3 Sample selection

There are a few ways to define UDGs in the literature. van Dokkum et al. (2015a,b) defined UDGs as the galaxies with $\mu_{0,B} > 24$ mag arcsec^{-2} and $r_e > 1.5$ kpc; some others used a slightly different quantity, the mean surface brightness within r_e, $\langle\mu\rangle_{e,r} \geq 24$ mag arcsec^{-2} (e.g. van der Burg et al. 2016; Yagi et al. 2016; Janssens et al. 2017). Given that the Sérsic indices, n, of most UDGs are around 1 (Koda et al. 2015; Román & Trujillo 2017a; Yagi et al. 2016) and colours $g - r \sim 0.6$ (van der Burg et al. 2016), $\langle\mu\rangle_{e,r} \geq 24$ mag arcsec^{-2} is approximately equivalent to g band $\mu_{0,g} > 23.5$ mag arcsec^{-2} (Graham & Driver 2005). In this work, we adopt the criteria as follows:

$$1.5 < r_e < 4.6\,\text{kpc},$$
$$-17 < M_g < -11.5\,\text{mag},$$
$$\text{and } \mu_{0,g} > 23.5\,\text{mag arcsec}^{-2},$$

where M_g is the g-band absolute magnitude.

We show the r_e–M_g relation for the model galaxies in Fig. 1 . Different mean surface brightness $\langle\mu\rangle_e$ thresholds are highlighted with the dotted lines. We find that almost all of the UDG candidates (red dots) are distributed above $\langle\mu\rangle_e = 25$ mag arcsec^{-2}. The luminosities of the observed UDGs are similar to those of the typical dwarf galaxies; however, their sizes are much larger. Interestingly, Fig. 1 shows that UDGs are not an isolated population, rather they exist as a continuous extension of typical dwarf galaxies. For galaxies of similar magnitudes, the UDGs occupy the large-sized tail of the size distribution, suggesting that UDGs are indeed a subsample of dwarf galaxies.

In order to understand the properties of UDGs and compare them with the typical dwarf galaxies more clearly, we select a counterpart sample of the dwarfs within the same luminosity range as the UDGs, but different sizes of $r_e \in (0.5, 1.0)$ kpc (Misgeld & Hilker 2011; van der Burg et al. 2016). According to the studies of Graham & Guzmán (2003) and Mo, van den Bosch & White (2010), these dwarf counterparts primarily include the dwarf ellipticals (dE) and dwarf spheroidals (dSph). Note that the ultracompact dwarfs are not included in this sample. In total, we have 4.4×10^4 UDGs and 1.3×10^5 dwarf counterparts, corresponding to 11 per cent and 32 per cent of the faint galaxies ($M_g \sim -17$ to -11.5), respectively, at $z = 0$ in MS-II.

3 UDGs IN SIMULATIONS AND OBSERVATIONS

In this section, we will first compare the properties of the model UDGs with the observations, and then explore how they vary with different environments.

3.1 UDGs in clusters

Most of the observed UDGs are discovered in clusters, e.g. in Coma (van Dokkum et al. 2015a), A168 (Román & Trujillo 2017a), A2744 (Janssens et al. 2017), and other eight low-redshift clusters (van der Burg et al. 2016, hereafter vdB16). Here, we focus on the comparison of the UDGs in clusters between the model predictions and observations.

Abundance. The abundances of UDGs are observed to correlate with the mass of their host cluster (van der Burg et al. 2016; Janssens et al. 2017): $N \propto M_{200}^{0.93\pm0.16}$, where N is the number of UDGs in a cluster and M_{200} is the cluster mass within a radius, r_{200}, within which the average density is 200 times the cosmic critical density. In Fig. 2, we show the observed results, as well as our model predictions on the abundances of UDGs as a function of their host cluster

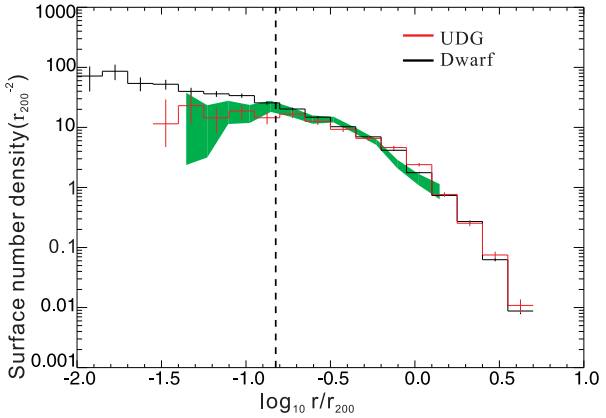

Figure 3. SND as a function of r/r_{200} for the model UDGs (red) and dwarf counterparts (black), respectively. The vertical dashed line denotes $r/r_{200} = 0.15$. The green component is the rescaled observed SND obtained by van der Burg et al. (2016).

masses. In order to compare with the observations directly, here we discard the model UDGs fainter than $\mu_{0,g} \sim 26.5$ mag arcsec^{-2} (approximately corresponding to the r band $\langle\mu\rangle_{e,r} \leq 27$ mag arcsec^{-2}). It shows that the model predictions are in excellent agreement with the observed abundance–mass relation, from groups to rich clusters.

Surface number density (SND) profile. Spatial distribution of the galaxies in clusters provides important clues to their evolution. In Fig. 3, we compare the SND profile of the observed UDGs in 8 observed clusters (van der Burg et al. 2016) with the average SND profile of the model UDGs in the 10 simulated clusters ($M_{200} > 10^{14}\,M_\odot\,h^{-1}$) selected from the MS-II simulation. The observed SND profile is rescaled by a constant factor to account for the different normalization methods. Clearly, the predicted SND profile fits very well with the observed one over all the observed scales from $0.03r_{200}$ to r_{200}, including the flatting feature in the inner part.

For completeness, we also show the SND profile of the typical dwarf counterparts (the black histogram) in Fig. 3. The SND of UDGs is similar to the profile of the dwarfs at $r/r_{200} > 0.15$ ($r/r_{200} = 0.15$ is denoted by the vertical dashed line in Fig. 3), while it is significantly lower at $r/r_{200} < 0.15$. Moreover, UDGs are absent in the innermost region $r/r_{200} < 0.03$. The lack of UDGs in the inner regions of clusters could be caused by two possible reasons: (i) UDGs might have been disrupted and dissociated by the strong tidal forces in the inner regions; (ii) UDGs might have fallen into the clusters more recently than the dwarf counterparts so that they have not arrived in the inner regions yet. Observationally, the evidence of tidal disruption for UDGs is very rare (Mihos et al. 2015; Toloba et al. 2016). We will show in Section 4 that our model indeed supports the second explanation.

Colour. Previous work found that except for certain UDGs in groups (e.g. Román & Trujillo 2017a), most of the observed UDGs are red (e.g. Koda et al. 2015; van Dokkum et al. 2015a; van der Burg et al. 2016). Fig. 4 displays the colour–magnitude diagrams for the model UDGs in our simulated clusters. Analogous to the observations, most of the model UDGs are red, except for several relatively faint ones. The left-hand panels show the colour distributions of the model UDGs (black histograms) and the 1σ range of the observed ones (coloured regions) in clusters (van Dokkum et al. 2015a; van der Burg et al. 2016). Most of the model UDGs are located at $g - r \sim 0.6 \pm 0.1$ and $g - i \sim 0.8 \pm 0.1$, in good agreement with the observations.

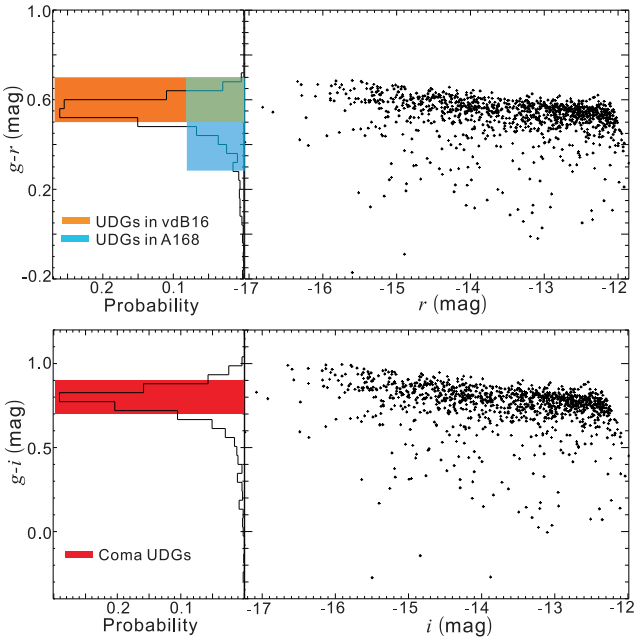

Figure 4. Distribution of colours and colour versus magnitude diagrams of the model UDGs in the clusters. The upper and lower panels show the $g - r$ colour versus the absolute r-band magnitudes, and $g - i$ colour versus i, respectively. The orange, blue and red components represent the approximate colour ranges of the observed UDGs in the eight low-redshift clusters (van der Burg et al. 2016), A168 (Román et al. 2017a) and Coma (van Dokkum et al. 2015a), respectively.

Morphology. Observationally, UDGs are found to have low Sérsic indices, $n \sim 0.6$–1 (e.g. Koda et al. 2015; Muñoz et al. 2015; van Dokkum et al. 2015a; van der Burg et al. 2016). Limited by the capability of semi-analytic models, we cannot measure the profiles directly. Instead, here we use the bulge-to-total mass ratio, B/T (Weinzirl et al. 2009), as a proxy, i.e. a lower Sérsic index corresponds to a lower value of B/T. The upper panel of Fig. 5 shows that most (95.7 per cent) of the model UDGs have extremely low B/T ($B/T < 0.1$), in line with the observed low Sérsic indices.

Most of our model UDGs present $B/T < 0.1$, suggesting that the model UDGs perhaps have an oblate, disc-like geometry. This result may conflict with the conclusion of Burkert (2017), who claimed that UDGs are more likely to be prolate rather than oblate because of their observed axial ratio range $q \sim 0.4$–1.0. However, this conflict may be due to the fact that most of the observed UDGs have relatively small inclination angles θ, i.e. they are more likely to be 'face-on' rather than 'edge-on'. This is because the UDGs with large inclination angles may be too bright to be identified as 'UDGs'. For instance, for a UDG with $\langle\mu\rangle_e \sim 26$ mag arcsec^{-2} and $\theta \sim 70^\circ$, its projected area decreases by a factor of $(\cos\theta)^2$, implying that the surface brightness changes about $2.5\log_{10}(\cos\theta)^2 \simeq 2.3$ mag; therefore, its apparent surface brightness becomes $\langle\mu\rangle_e \sim 23.7$ mag arcsec^{-2}, which would be beyond the criterion to select UDGs.

Total mass. The observed UDGs are very diffuse, and can reside in the dense environments without significant evidence of tidal disruption, suggesting that they are highly dark-matter-dominated systems. Observationally, we usually use the abundance of the member globular clusters to infer UDG virial mass, m_{vir}. In the lower panel of Fig. 5, we show the distribution of the virial masses of the model UDGs. Most of them are in the range of 10^9–$10^{11}\,M_\odot$, consistent with the recently reported total masses for VCC 1287,

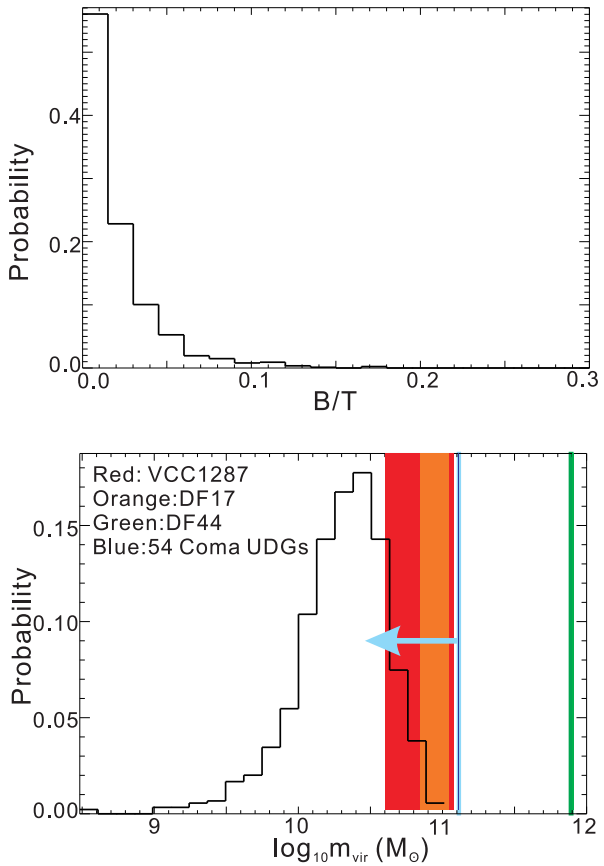

Figure 5. Distribution of B/T (the upper panel) and $m_{\rm vir}$ (the lower panel) for model UDGs in the clusters, respectively. The coloured components denote the virial masses and their errors of some observed UDGs. The arrow indicates upper limit of that the virial masses of the 54 Coma UDG candidates.

DF17 and UGC2162 (Beasley & Trujillo 2016; Beasley et al. 2016; Trujillo et al. 2017), and Fornax UDGs (Zaritsky 2017) as well as 54 Coma UDGs (Amorisco et al. 2016). The peak of the model predictions is lower than the observations, which is primarily because that the measured UDGs are observationally brighter. Note that one particular case, DF44, is reported (van Dokkum et al. 2016) to be hosted in a dark halo as massive as $m_{\rm vir} \sim 8 \times 10^{11}\,{\rm M}_{\odot}$, an order of magnitude more massive than the typical mass found for the other UDG hosts. Zaritsky (2016) argued that DF44 lies at the upper-end in the size-enclosed mass relation of the observed UDGs and thus may not be a typical UDG.

3.2 UDGs in the Local Group and Local Volume

Most UDGs are discovered in rich clusters and their surroundings. A very interesting issue is whether UDGs could exist in the Local Group ($\sim 5 \times 10^{12}\,{\rm M}_{\odot}$; e.g. Li & White 2008). In the literature, two UDG candidates are found in the census of faint galaxies in the Local Group: Sagittarius dSph (McConnachie 2012) and Andromeda XXXII (Martin et al. 2013). Sagittarius dSph is 26 kpc away from us, with V-band absolute magnitude of $M_V = -13.5$ mag, $r_{\rm e} = 2.6$ kpc, and V-band $\mu_0 \simeq 25.2$ mag arcsec^{-2}. This UDG candidate has been reported by Yagi et al. (2016), who are the first authors to identify UDGs in the Local Group. Andromeda XXXII is 0.78 Mpc away from us, with $M_V = -12.3$, $r_{\rm e} = 1.46$ kpc (slightly smaller than 1.5 kpc), and $\mu_0 = 26.4$ mag arcsec^{-2}.

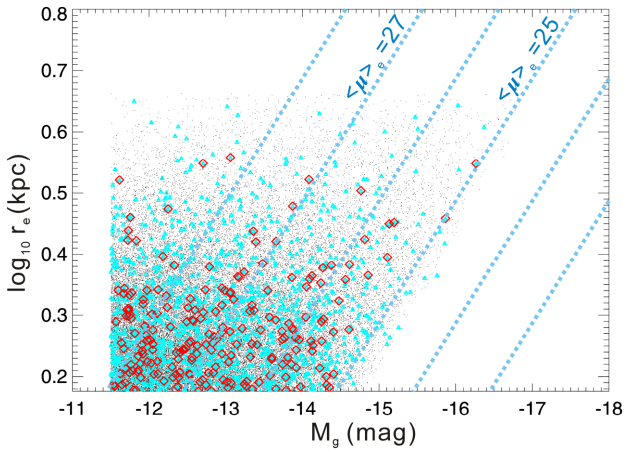

Figure 6. $r_{\rm e}$–M_g relation for UDGs in the Local Group and in the Local Volume. Black points denote all of the model UDGs selected in Section 2.3. Red diamonds and cyan triangles denote the UDGs in the Local Groups and the Local Volumes analogue, respectively. Analogous to Fig. 1, the blue dotted lines highlight $\langle\mu\rangle_{\rm e} \simeq 23 \sim 28$ mag arcsec^{-2}.

To compare the model predictions with the data, we first define the Local Group analogues in the simulation according to the observable properties of the Local Group. Here, we adopt the selection criteria similar to those described in Xie, Gao & Guo (2014). We first select the Milky Way analogue using the criteria: $B/T < 0.5$ and $5.4 \times 10^{10} < M_{\rm MW} < 7.4 \times 10^{10}\,{\rm M}_{\odot}$, where $M_{\rm MW}$ is the stellar mass of the Milky Way analogue, and then request that there is only one bright companion (M31 analogue) within 1 Mpc from each Milky Way analogue, with stellar mass $M_{\rm MW} < m_{\rm st} < 2M_{\rm MW}$ (this mass restriction is slightly different from the criterion used in Xie et al. 2014). We further require no galaxy clusters with masses $\geq 10^{14}\,{\rm M}_{\odot}$ within 10 Mpc of the Local Group catalogue. In total, we find 69 'Local Group' analogues in the model galaxy catalogue. 207 model UDGs are found within 1 Mpc of the 69 'Local Group' analogues, i.e. three UDGs in each system on average. The $r_{\rm e}$ versus M_g relation of these 207 UDGs are overplotted with the red diamonds in Fig. 6.

We further extend the searching radius from 1 to 5 Mpc as the Local Volume analogue. There are in total 1654 model UDGs (cyan triangles in Fig. 6) in the simulated Local Volumes, corresponding to 24 UDGs in each system. Observationally, we use the dwarf catalogue by Karachentsev, Makarov & Kaisina (2013)[1] to search for the UDG candidates and find 23 possible UDGs residing in the Local Volume, as listed in Table 1. Note that these galaxies are observed in a different wavelength and their μ_0 are not given by Karachentsev et al. (2013), we thus use the selection criteria slightly different from those in Section 2.3 by requiring: a linear Holmberg diameter $A_{26} > 3$ kpc, $\langle\mu\rangle_B \geq 25$ mag arcsec^{-2}, and $10^6 < L_K < 10^9\,{\rm L}_{\odot}$. Among these possible UDG candidates, CenA-MM-Dw3 has been reported (Crnojević et al. 2016).

In summary, the predicted abundances of UDGs in the simulated Local Group analogues and Local Volume analogues agree very well with those in the real Universe. In addition, we find that the model UDGs comprise less than 10 per cent of the total faint populations ($M_g \sim -17$ to -11.5 mag) in these two systems and thus will

[1] http://www.sao.ru/lv/lvgdb/

Table 1. Parameters of the 23 UDG candidates selected from the dwarf catalogue of Karachentsev et al. (2013). Column (1): dwarf Name. Column (2): distance (Mpc) to the Milky Way. Column (3): the linear Holmberg diameter in unit of kpc (Karachentsev et al. 2004, 2013). Column (4): *B*-band absolute magnitude. Column (5): mean surface brightness. Column (6): logarithm of *K*-band luminosity ($L_\odot$).

Name Col. (1)	D Col. (2)	A_{26} Col. (3)	M_B Col. (4)	$\langle\mu\rangle_B$ Col. (5)	$\log L_K$ Col. (6)
Sag dSph	0.02	3.08	−12.67	26.08	8.02
And XXXII	0.78	3.60	−11.53	27.56	7.56
NGC3109	1.34	7.73	−15.75	25.01	8.58
DDO099	2.65	3.24	−13.53	25.34	7.42
KK35	3.16	3.91	−14.30	25.00	7.97
KKH12	3.48	3.44	−13.35	25.65	7.80
MB3	3.48	5.19	−13.97	25.92	8.22
Cam A	3.56	4.61	−13.85	25.78	7.79
CenA-MM-Dw1	3.63	3.13	−12.56	26.23	7.98
IKN	3.75	3.15	−11.63	27.17	7.60
ESO269-058	3.75	5.52	−15.04	25.00	8.86
KK77	3.80	3.15	−12.22	26.58	7.84
HolmIX	3.85	3.15	−13.75	25.06	7.75
HolmI	4.02	5.54	−14.59	25.44	8.05
LV J1228+4358	4.07	4.56	−13.94	25.67	7.83
UGC A442	4.37	7.52	−14.71	25.98	8.03
DDO169	4.41	3.65	−13.80	25.32	7.73
IC3687	4.57	6.92	−14.60	25.91	8.19
CenA-MM-Dw3	4.61	6.63	−12.32	28.10	7.88
DDO226	4.92	3.12	−13.63	25.15	7.71
DDO126	4.97	4.14	−14.42	25.00	8.09
KK208	5.01	8.77	−14.39	26.64	8.71
ESO115-021	5.08	10.14	−15.58	25.76	8.75

not significantly affect the corresponding conditional luminosity functions by including/excluding UDGs.

4 DISTRIBUTION OF THE UDGs IN THE UNIVERSE

In the last section, we demonstrated that the model reproduces most of the available observational properties of UDGs. This encourages us to use our model to make prediction of the distribution of UDGs in the Universe.

Fig. 7 shows the accumulative fraction of the model UDGs as a function of the group masses. We find that only 4 per cent model UDGs reside in the clusters more massive than $10^{14}\,M_\odot$, while most of the model UDGs (80 per cent) reside in the groups with $M_{200} < 10^{12}\,M_\odot$ or in the fields. We further find that most of the model UDGs are red in colour regardless of their environments, yet with an expected positive correlation between the red fractions and densities of environments.

Comparing the distributions of the model dwarf galaxies and UDGs, in the clusters and groups (more massive than $10^{12}\,M_\odot$), 7 per cent of the dwarf galaxies are classified as UDGs, and the fraction is nearly independent of the host halo mass. However in the fields, this fraction is as high as 14 per cent, suggesting that UDGs tend to stay in the lower density environment. The general low fractions of UDGs also suggest that the luminosity function at the faint end will not be significantly affected by including/excluding UDGs; the effect of UDGs on the conditional luminosity functions is even weaker in the groups and clusters.

In order to study the environmental dependence of the model UDGs in more details, we further divide the model UDGs into

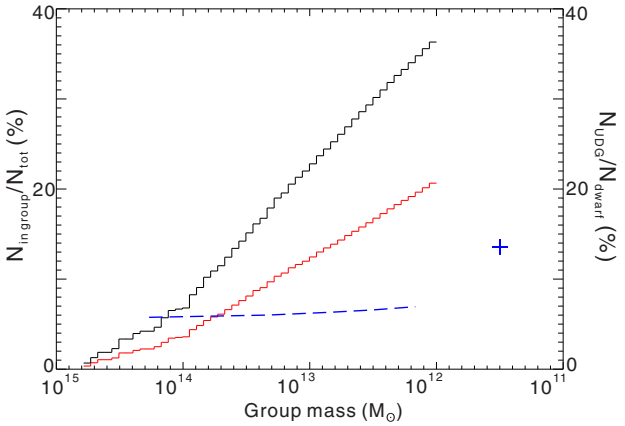

Figure 7. Solid histograms show the cumulative fractions of the model UDGs (red) and dwarfs (black) in groups with the different masses (left *y* axis). Dashed curve shows the ratio between the abundances of the model UDGs and dwarfs as a function of the host group mass (right *y* axis). The blue cross marks the ratio in the fields.

four subsamples according to their host halo masses, clusters ($m \geq 10^{14}\,M_\odot\,h^{-1}$), groups ($m \sim 10^{12}$–$10^{14}\,M_\odot\,h^{-1}$), galaxy systems ($m < 10^{12}\,M_\odot\,h^{-1}$) and fields. UDGs in the former three systems exist as satellite galaxies, while in the fields, they are central galaxies of their own haloes (i.e. isolated UDGs). In Fig. 8, we show the probability distributions of six different physical properties for the four UDG subsamples. The stellar masses, m_{st}, of the model UDGs increase with the densities of environments (panel A), e.g. m_{st} of the UDGs in the clusters is higher by about 0.2 dex than those in the fields. This is consistent with the increasing fraction of the red populations with the increasing environmental density, as the red galaxies are usually older and more massive (for a given luminosity). UDGs in clusters tend to have lower specific star formation rates (SSFR = star formation rate/m_{st}; panel F) and be relatively older (panel D). Galaxies formed earlier (with higher mass-weighted-ages, τ) are usually more compact, which is reflected by the distributions of r_e (panel E). Different from the other properties, dependences of the virial mass m_{vir} (panel B) and morphology (panel C) on the environments are very weak. Regardless of the environments, most of the model UDGs are disc-dominated systems and are formed in the haloes of virial mass $\sim 10^{10}\,M_\odot$, very similar to that of a typical dwarf galaxy.

5 FORMATION OF UDGs

As discussed above, our model predicts that UDGs have the similar dark matter haloes to those of the typical dwarf galaxies. In this section, we explore why the stellar components of UDGs are so extended.

In order to investigate the differences between the model UDGs and typical dwarf galaxies more clearly, in Fig. 9 we compare the distributions of the stellar mass (panel A), stellar mass-to-light ratio (panel B), B/T (panel C) and host halo mass (panel D) between the two samples. The typical dwarfs in general have larger stellar masses than UDGs (panel A). This is primarily because that the model UDGs are younger (see the lower panel in Fig. 10) and bluer. Consistently, the stellar mass-to-light ratio of a UDG is typically smaller than that of a typical dwarf galaxy by around 50 per cent (panel B). One needs to pay particular attention when converting the luminosities of UDGs to their stellar masses. UDGs are much more extended than the regular dwarf galaxies, and thus we expect that

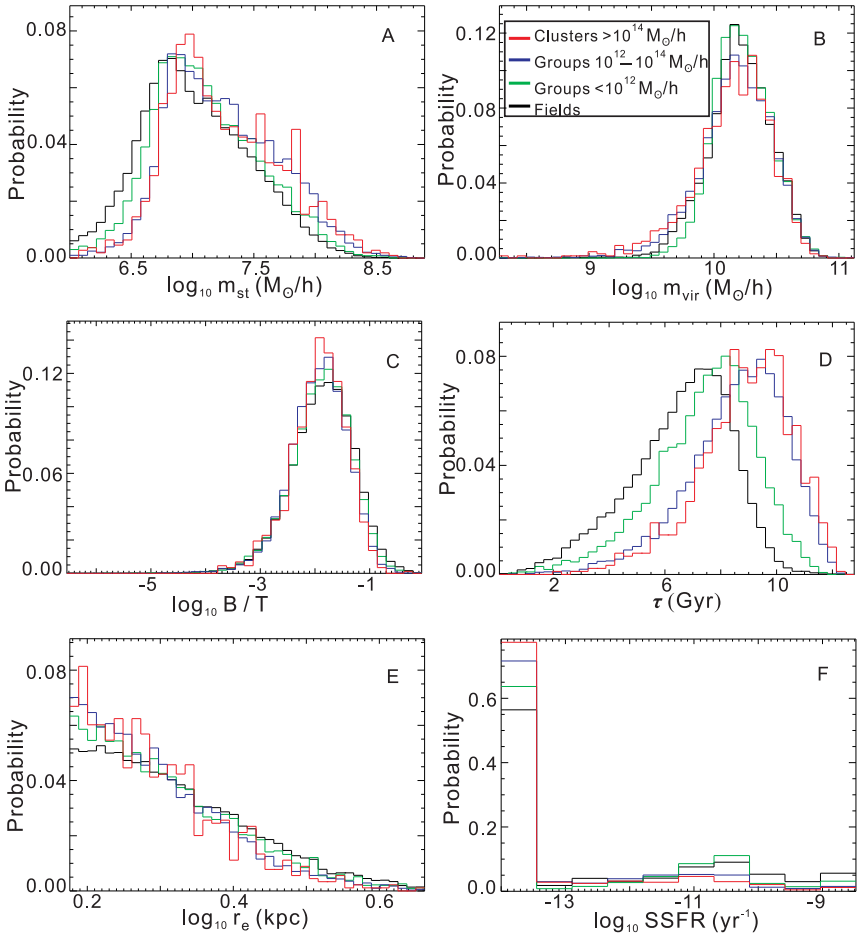

Figure 8. A–F panels show the distributions of $m_{\rm st}$, $m_{\rm vir}$, B/T, τ, $r_{\rm e}$ and SSFR, respectively. The red, blue, green and black histograms denote the UDGs in clusters ($m \geq 10^{14}\,{\rm M}_{\odot}\,h^{-1}$), in groups ($m \sim 10^{12}$–$10^{14}\,{\rm M}_{\odot}\,h^{-1}$), in galaxy systems ($m < 10^{12}\,{\rm M}_{\odot}\,h^{-1}$) and in fields, respectively.

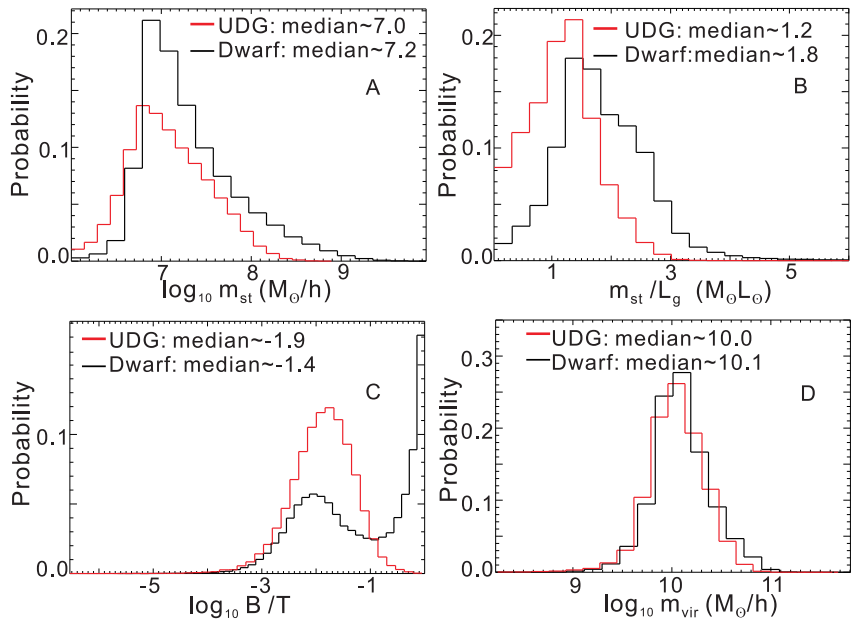

Figure 9. A–D panels show the distributions of $m_{\rm st}$, $m_{\rm st}/L_g$, B/T and $m_{\rm vir}$, respectively. Red and black histograms represent the distribution of UDGs and their dwarf counterparts, respectively. The median values of each quantity are shown in the corresponding panel.

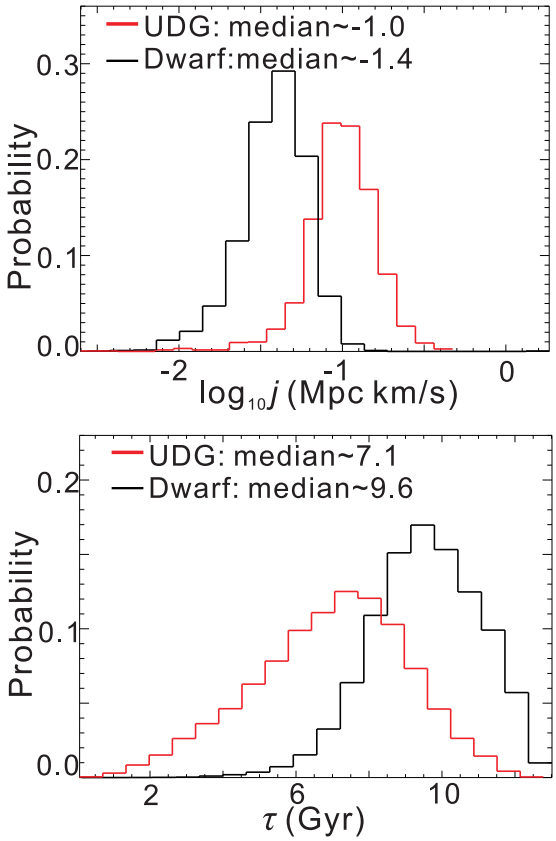

Figure 10. The distributions of the specific angular momenta j of the progenitor haloes (upper panel) at $t_{\rm half}$ and galactic ages τ (lower panel) for the model UDGs (red histogram) and dwarf counterparts (black histogram), respectively.

the internal structures of UDGs differ from the dwarf counterparts as well. As shown in the panel C, B/T of the model UDGs are significantly lower than those of the typical dwarf counterparts. 96.6 per cent of the model UDGs present $B/T < 0.1$; whereas about 27 per cent of the dwarf counterparts are dEs with $B/T > 0.5$. Regardless of the differences shown above, the distributions of the virial masses, $m_{\rm vir}$, of the model UDGs and dwarf counterparts are very similar to each other. The host haloes of UDGs are only slightly less massive than those of their dwarf counterparts by 0.1 dex.

There are two reasons that may account for the unique feature of UDGs: (1) UDGs may form much later than the typical dwarfs, since the objects formed later are usually more extended because of the diluted Universe at a low redshift; (2) UDGs may have much higher spin parameters as naively expected from the standard galaxy formation scenario in which the galaxy size $r_{\rm e} \propto \lambda R_{\rm vir}$ (e.g. Mo et al. 1998; Amorisco & Loeb 2016), where λ and $R_{\rm vir}$ are the spin parameter and the virial radius of the host halo, respectively. We will examine these below with our model. Note that in the modern galaxy formation models, e.g. Guo11 and Bower et al. (2010), the size of a present galaxy is not uniquely determined by the spin parameter of its host halo at $z = 0$ or any specific redshift, rather it is a cumulative consequence of the angular momentum evolution of its parent halo and star formation. The size of a galaxy is largely determined by the rotational states of its host halo when the galactic star formation rate was high. We use the specific angular momentum of the main progenitor of a halo at the epoch ($t_{\rm half}$) when half of its stellar mass was assembled to take into account this integral

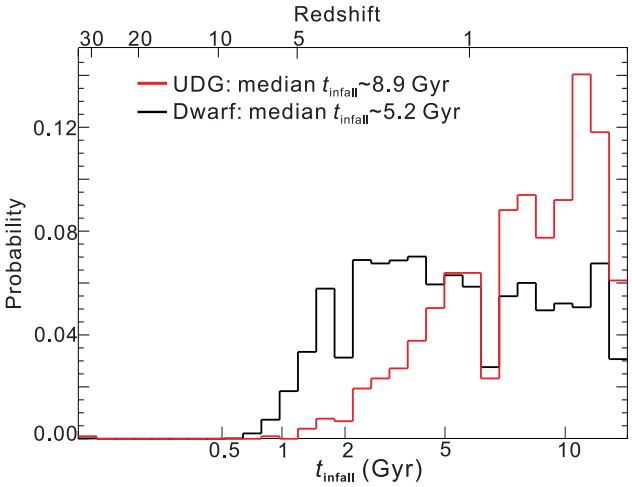

Figure 11. Distributions of $t_{\rm infall}$ for the UDGs (red) and their dwarf counterparts (black) in the clusters, respectively.

effect. Note, the exact choice of the redshift only changes our result quantitatively but not qualitatively.

In Fig. 10, we present the distributions of the specific angular momenta j of the progenitor haloes at $t_{\rm half}$ and galaxy ages τ for the model UDGs and dwarf counterparts. Clearly, compared with the typical dwarfs, the specific angular momenta of the model UDGs are larger by a factor of 2.5 at $t_{\rm half}$. Also as shown in the lower panel of Fig. 10, the UDGs are indeed much younger with a median age of 7.1 Gyr, compared with the typical dwarfs that have a median age of 9.6 Gyr. Further, these suggest that it is indeed the combination of the late formation of UDGs and high spins of the host haloes that result in the large sizes of UDGs. Therefore, the high-spin tail origin of UDGs proposed by Amorisco & Loeb (2016) is not the complete story to explain the formation of UDGs. Besides, we find that almost all of the model UDGs in the clusters fall in directly from the field.

Di Cintio et al. (2017) developed an alternative strong-outflow model to explain the extended sizes of UDGs. Although this model can also reproduce the broad colour range and low Sérsic indices of observed UDGs, their simulated UDGs do not live in particularly high-spin haloes, which conflicts with both of our model prediction and the recent observational spin parameters of UDGs from the ALFALFA H I survey (Leisman et al. 2017). Besides, their simulation contains about 40 galaxies with halo masses of 10^{10}–10^{11} $M_\odot$ (Wang et al. 2015), among which 8–21 (depending on the effective radius threshold $r_{\rm e} = 1$ or 2 kpc) of them are UDGs, suggesting a much higher fraction of UDGs than our model prediction; in the sense that the outflow model may overestimate the abundance of UDGs.

Another interesting phenomenon is that the number density profile of UDGs is flat towards the centre in the observed clusters, quite different from that of the typical dwarfs. One possible reason may be that the UDGs fell into the clusters later than the typical dwarfs. We illustrate it in Fig. 11 by comparing the distributions of the infall-time $t_{\rm infall}$ (the time at which a galaxy was accreted into a cluster; $t_{\rm infall} \simeq 13.75$ Gyr corresponding to $z = 0$) of the two dwarf populations in the 10 simulated clusters. As expected, the infall-time of the model UDGs is on average significantly later than that of the dwarf counterparts, with a median value of $\langle t_{\rm infall} \rangle \sim 8.9$ Gyr and $\langle t_{\rm infall} \rangle \sim 5.2$ Gyr for the model UDGs and dwarf counterparts, respectively. Therefore, the lack of UDGs in the

inner regions of clusters as shown in Fig. 3, as well as lack of the tidal disruption features in observations are the natural consequences of this late infall-time.

6 CONCLUSION AND DISCUSSION

As a special subset of low surface brightness population, UDGs draw much attention recently because they are as faint as the typical dwarf galaxies, yet have the sizes similar to those of the L^* galaxies. The origin of UDGs is a mystery: are they the genuine dwarf galaxies with extremely large sizes or failed L^* galaxies?

We use galaxy formation models (Guo11; Guo et al. 2013) to study this special galaxy population. The predicted properties of UDGs in the clusters and groups (where most of the UDGs are discovered) agree very well with the observational results, including the abundance, number density profile, colour distribution and morphology. Our model predicts about 4 and 24 UDG candidates in the Local Group and Local Volume analogues, respectively. When searching for such candidates in the Local Group and Local Volume with existing observational data, we find that the numbers of UDGs in these two systems agree remarkably well with the model predictions.

We demonstrate that UDGs are genuine dwarf galaxies and can naturally emerge from the ΛCDM model. It is the combination of the later formation of UDGs and the relatively larger spins of their host haloes that results in the more extended feature of this particular population. The lack of UDG candidates in the inner regions of clusters and the lack of tidal disruption features can be naturally explained by the later infall of the UDGs.

Compared to the typical dwarf galaxies, UDGs tend to reside in the low-density regions consistent with their later formation. However, in the fields where there is no environmental effect, UDGs are redder than the typical dwarf galaxies. This is because the UDGs are more extended and the star formation ceases when the densities of the gas discs drop below a certain threshold. The red colours of UDGs suggest that it is even harder to detect UDGs than the typical dwarf galaxies. Fortunately, the model predicts only 7 per cent of dwarf galaxies in clusters and 14 per cent in fields are identified as UDGs, suggesting that it will not significantly affect the global luminosity function at the faint end, nor the conditional luminosity functions. Although most of UDGs are discovered in dense environments, we anticipate to discover a much higher fraction in underdense regions in the future.

ACKNOWLEDGEMENTS

We thank Professor Karachentsev I. D. for his helpful discussion on the UDG candidates in the Local Volume. QG and LG acknowledge support from NSFC grants (no. 11425312), and two Newton Advanced Fellowships, as well as the hospitality of the Institute for Computational Cosmology at Durham University. THP acknowledges support in form of the FONDECYT Regular Project no. 1161817 and by the BASAL Center for Astrophysics and Associated Technologies (PFB-06). JP acknowledges support from the National Basic Research Program of China (program 973 under grant no. 2015CB857001) and NSFC under grant no. 11573030.

REFERENCES

Amorisco N. C., Loeb A., 2016, MNRAS, 459, L51
Amorisco N. C., Monachesi A., White S. D. M., 2016, preprint (arXiv:1610.1595)
Beasley M. A., Trujillo I., 2016, ApJ, 830, 23
Beasley M. A., Romanowsky A. J., Pota V., Navarro I. M., Delgado D. M., Neyer F., Deich A. L., 2016, ApJ, 819, L20
Bower R. G., Vernon I., Goldstein M., Benson A. J., Lacey C. G., Baugh C. M., Cole S., Frenk C. S., 2010, MNRAS, 407, 2017
Boylan-Kolchin M., Springel V., White S. D. M., Jenkins A., Lemson G., 2009, MNRAS, 398, 1150
Bruzual G., Charlot S., 2003, MNRAS, 344, 1000
Burkert A., 2017, ApJ, 838, 93
Colless M. et al., 2001, MNRAS, 328, 1039
Conroy C., Wechsler R. H., 2009, ApJ, 696, 620
Crnojević D. et al., 2016, ApJ, 823, 19
Dalcanton J. J., Spergel D. N., Gunn J. E., Schmidt M., Schneider D. P., 1997a, AJ, 114, 635
Dalcanton J. J., Spergel D. N., Summers F. J., 1997b, ApJ, 482, 659
Davis M., Efstathiou G., Frenk C. S., White S. D. M., 1985, ApJ, 292, 371
De Lucia G., Blaizot J., 2007, MNRAS, 375, 2
Di Cintio A., Brook C. B., Dutton A. A., Macciò A. V., Obreja A. C., Dekel A., 2017, MNRAS, 466, L1
Gao L., Navarro J. F., Frenk C. S., Jenkins A., Springel V., White S. D. M., 2012, MNRAS, 425, 2169
Graham A. W., Driver S. P., 2005, Publ. Astron. Soc. Aust., 22, 118
Graham A. W., Guzmán R., 2003, AJ, 125, 2936
Guo Q., White S., Li C., Boylan-Kolchin M., 2010, MNRAS, 404, 1111
Guo Q. et al., 2011, MNRAS, 413, 101
Guo Q. et al., 2013, MNRAS, 435, 897
Harris W. E., Harris G. L. H., Alessi M., 2013, ApJ, 772, 82
Harris W. E., Harris G. L., Hudson M. J., 2015, ApJ, 806, 36
Huang S., Haynes M. P., Giovanelli R., Brinchmann J., 2012, MNRAS, 756, 113
Jaffe W., 1983, MNRAS, 202, 995
Janssens S., Abraham R., Brodie J., Forbes D., Romanowsky A. J., van Dokkum P., 2017, ApJ, 839, L17
Karachentsev I. D., Karachentseva V. E., Huchtmeier W. K., Makarov D. I., 2004, ApJ, 127, 2031
Karachentsev I. D., Makarov D. I., Kaisina E. I., 2013, AJ, 145, 101
Koda J., Yagi M., Yamanoi H., Komiyama Y., 2015, ApJ, 807, L2
Leisman L. et al., 2017, preprint (arXiv:1703.05293)
Li Y.-S., White S. D. M., 2008, MNRAS, 384, 1459
McConnachie A. W., 2012, ApJ, 144, 4
Makarov D. I., Sharina M. E., Karachentseva V. E., Karachentsev I. D., 2015, A&A, 581, 82
Martin N. F. et al., 2013, ApJ, 772, 15
Martínez-Delgado D. et al., 2016, AJ, 151, 96
Mihos J. C. et al., 2015, ApJ, 809, L21
Misgeld I., Hilker M., 2011, MNRAS, 414, 3699
Mo H., Mao S., White S. D. M., 1998, MNRAS, 295, 319
Mo H., van den Bosch F., White S., 2010, Galaxy Formation and Evolution. Cambridge Univ. Press, Cambridge
Muñoz R. P. et al., 2015, ApJ, 813, L15
Nierenberg A. M., Auger M. W., Treu T., Marshall P. J., Fassnacht C. D., Busha M. T., 2012, ApJ, 752, 99
Okamoto T., Gao L., Theuns T., 2008, MNRAS, 390, 920
Peng E. W., Sungsoon L., 2016, ApJ, 822, L31
Román J., Trujillo I., 2017a, MNRAS, 468, 703
Román J., Trujillo I., 2017b, MNRAS, 468, 703
Scannapieco C., Tissera P. B., White S. D. M., Springel V., 2008, MNRAS, 389, 1137
Simha V., Weinberg D. H., Davé R., Fardal M., Katz N., Oppenheimer B. D., 2012, MNRAS, 423, 3458
Springel V., White S. D. M., Tormen G., Kauffmann G., 2001, MNRAS, 328, 726
Spergel D. et al., 2003, ApJS, 148, 175
Springel V. et al., 2005, Nature, 435, 629
Stinson G. S., Brook C., Macciò A. V., Wadsley J., Quinn T. R., 2013, MNRAS, 428, 129
Toloba E. et al., 2016, ApJ, 2016, 816, L5

Trujillo I., Román J., Filho M., Sánchez Almeida J., 2017, ApJ, 836, 191
Trujillo-Gomez S., Klypin A., Colín P., Ceverino D., Arraki K. S., Primack J., 2015, MNRAS, 446, 1140
van der Burg R. F. J., Muzzin A., Hoekstra H., 2016, A&A, 590, 20
van Dokkum P. G., Abraham R., Merritt A., Zhang J., Geha M., Conroy C., 2015a, ApJ, 798, L45
van Dokkum P. G. et al., 2015b, ApJ, 804, L26
van Dokkum P. G. et al., 2016, ApJ, 828, 6
Wang L., Dutton A. A., Stinson G. S., Macciò A. V., Penzo C., Kang X., Keller B. W., Wadsley J., 2015, MNRAS, 454, 83
Weinzirl T., Jogee S., Khochfar S., Burkert A., Kormendy J., 2009, ApJ, 696, 411
Xie L., Gao L., Guo Q., 2014, MNRAS, 441, 933
Xie L., Guo Q., Cooper A. P., Frenk C. S., Li R., 2015, MNRAS, 447, 636
Yagi M., Koda J., Komiyama Y., Yamanoi H., 2016, ApJS, 225, 11
Yozin C., Bekki K., 2015, MNRAS, 452, 937
Zaritsky D., 2017, MNRAS, 464L, 110

This paper has been typeset from a TEX/LATEX file prepared by the author.